ARTICLE

Physiologically Based Pharmacokinetic Models for Adults and Children Reveal a Role of Intracellular Tubulin Binding in Vincristine Disposition

Christine M. Lee[1], Nicole R. Zane[2], Gareth Veal[3] and Dhiren R. Thakker[1],*

Vincristine is a cytotoxic chemotherapeutic agent used as first-line therapy for pediatric acute lymphocytic leukemia. It is cleared by hepatic oxidative metabolism by CYP3A4 and CYP3A5 and via hepatic (biliary) efflux mediated by P-glycoprotein (P-gp) transporter. Bottom-up physiologically based pharmacokinetic (PBPK) models were developed to predict vincristine disposition in pediatric and adult populations. The models incorporated physicochemical properties, metabolism by CYP3A4/5, efflux by P-gp, and intracellular binding to β-tubulin. The adult and pediatric PBPK models predicted pharmacokinetics (PK) within twofold of the observed PK parameters (area under the curve, terminal half-life, volume of distribution, and clearance). Simulating a higher hypothetical (4.9-fold) pediatric expression of β-tubulin relative to adult improved predictions of vincristine PKs. To our knowledge, this is the first time that intracellular binding has been incorporated into a pediatric PBPK model. Utilizing this PBPK modeling approach, safe and effective doses of vincristine could be predicted.

Study Highlights

WHAT IS THE CURRENT KNOWLEDGE ON THE TOPIC?
☑ Vincristine, a first-line treatment for pediatric cancer, is cleared by hepatic oxidative metabolism by CYP3A4 and CYP3A5 and via hepatic efflux mediated by P-glycoprotein (P-gp) transporter.

WHAT QUESTION DID THIS STUDY ADDRESS?
☑ The objective of the current study was to develop mechanistic physiologically based pharmacokinetic (PBPK) models to predict the vincristine disposition of vincristine following i.v. administration to adults and children.

WHAT DOES THIS STUDY ADD TO OUR KNOWLEDGE?
☑ The mechanistic PBPK models predict vincristine PK upon i.v. administration in adults and children. The models suggest that CYP3A5 and P-gp do not seem to play a significant role in the clearance of vincristine in adults or children. Interestingly, intracellular binding of vincristine to β-tubulin is a key parameter in the PBPK models for predicting the distribution phase of vincristine PK, and there may be age-related differences in the extent of intracellular binding to β-tubulin.

HOW MIGHT THIS CHANGE DRUG DISCOVERY, DEVELOPMENT, AND/OR THERAPEUTICS?
☑ These PBPK models provide a useful tool to investigate the relationship between vincristine exposure and clinical outcomes without invasive monitoring of plasma drug concentrations.

The vinca alkaloid vincristine is a chemotherapeutic agent used as first-line therapy for pediatric acute lymphocytic leukemia (ALL) and acute myeloid leukemia. ALL is the most common pediatric cancer, accounting for 26% of cancer diagnosed in children up to 14 years of age. Younger children are disproportionately affected by ALL, with the highest incidence in children 2–5 years old.[1,2] Vincristine is also an important anticancer agent in other adult and pediatric cancers, including Wilms tumor, Hodgkin disease, and non-Hodgkin lymphoma.[3] Vincristine disrupts mitosis by binding to the β-tubulin subunits of intracellular microtubule structures. This antimitotic effect is also responsible for its dose-limiting toxicity of peripheral neuropathy, often manifested by tingling, numbness, a burning sensation, and muscle weakness.[4]

Understanding the relationship between vincristine drug pharmacokinetics (PK) and risk of peripheral neuropathy is limited by sparse availability of clinical PK data.[3] Increased risk of peripheral neuropathy has been reported in pediatric patients with reduced vincristine clearance, although systemic exposure to vincristine has not been correlated with vincristine neurotoxicity.[5,6] However, other studies indicate that clinical outcomes in children with ALL are related to the clearance and exposure of vincristine.[7] Significant neurotoxicity in pediatric patients has been observed when vincristine is coadministered with azole antifungals, which are potent

CYP3A inhibitors (e.g., itraconazole and voriconazole), thereby increasing vincristine exposure.[8] Nutritional status may also impact clinical outcomes and neurotoxicity risk by affecting clearance of the drug and hence exposure to it; in pediatric patients with Wilms tumor and malnutrition, decreased vincristine clearance (CL) and a twofold increase in exposure (area under the curve (AUC)) has been observed compared with pediatric patients without malnutrition.[9]

Pediatric PK data for vincristine are limited despite a long history of use in pediatric cancer. As a cytotoxic agent, vincristine is unlikely to be administered to healthy volunteers for prediction of vincristine PK or drug–drug interactions. Therefore, understanding and predicting the potential age-related impact on vincristine disposition is essential for informing proper dosing and treating pediatric patients with cancer.

The objective of the current study was to develop physiologically based pharmacokinetic (PBPK) models to predict the disposition of vincristine following i.v. administration to adults and children. Previously, we have developed bottom-up PBPK models for pediatric disposition of voriconazole and sildenafil, which are both predominantly cleared via hepatic oxidative metabolism.[10,11] Like voriconazole and sildenafil, vincristine is metabolized by CYP3A4. Its clearance in infants and children, when normalized to body surface area or body weight, is higher than in adults, despite decreased CYP3A4 expression and activity in children.[5,12,13] In contrast to voriconazole and sildenafil, vincristine is preferentially metabolized by the genetically polymorphic enzyme CYP3A5, and it undergoes biliary excretion via P-glycoprotein (P-gp; also known as MDR1), a hepatic efflux transporter that is expressed at ~60% and 80% of adult levels in infants and children, respectively.[14] Pediatric patients who are high expressers of CYP3A5 have higher metabolite plasma concentrations and lower incidence of peripheral neuropathy vs. low expressers.[6] A similar approach could be applied to vincristine to predict its disposition in adults and children and thus assist in providing safe and effective dosing of this drug with a narrow therapeutic window.

METHODS

Materials
[³H]-Vincristine was purchased from American Radiolabeled Chemicals (St. Louis, MO). GW918 was a gift from GlaxoSmithKline (Research Triangle Park, NC). Madin-Darby canine kidney strain II cells, expressing human P-gp after transfection with human MDR1 complementary DNA (MDCKII-MDR1), were obtained from the Netherlands Cancer Institute (Amsterdam, The Netherlands).

Cell culture
MDCKII-MDR1 cells were seeded at a density of 100,000 cells/cm^2 on 12-well Transwell plates (Corning, Corning, NY) and maintained in a CO_2 incubator at 37°C. Cell monolayers were used for experiments 6 days after seeding.

Transport studies
To obtain estimates of apparent Michaelis-Menten constant (K_m) and maximal flux (J_{max}) for P-gp-mediated apical (AP)

efflux of vincristine, *in vitro* transport studies were conducted with MDCKII-MDR1 cell monolayers overexpressing P-gp, as previously described.[15] Monolayers were incubated in transport buffer (pH 7.4) at 37°C. Dose solutions were added to the AP compartment for absorptive transport and basolateral (BL) compartment for secretory transport. To determine the transport of vincristine in the absence of P-gp activity (e.g., approximating conditions of permeability due to passive diffusion),[16] the P-gp inhibitor GW918 (1 μM) was included and transport determined. Samples were analyzed by liquid scintillation spectrometry. Calculation of apparent J_{max} and K_m parameters for P-gp-mediated efflux of vincristine were performed, as previously described, using nonlinear regression analyses (GraphPad Prism 7, La Jolla, CA).[15]

Pharmacokinetic data
Individual adult vincristine concentration-time data were obtained by digitizing published PK profiles (GetData Graph Digitizer, version 2.26).[17–19] Pediatric vincristine concentration-time data were obtained from a PK study of 25 patients with localized Wilms tumors, with ages ranging from 5 months to 9 years. Samples were analyzed at Newcastle University (UK) using a validated liquid chromatography-mass spectrometry assay, as described previously.[9] A subset of these concentration-time data has previously been published.[9] Pediatric concentrations were dose-normalized to account for the range of doses given (0.3–1.8 mg). Noncompartmental analysis was performed on the digitized adult concentration data and the pediatric concentration data using Phoenix 8.0 (Certara USA, Inc., Princeton, NJ).

PBPK model and simulation
A whole-body adult PBPK model was first developed using PK-Sim software (Open Systems Pharmacology Suite, version 7.1) that incorporated vincristine physicochemical parameters (**Table 1**). Population-based PK simulations were performed for virtual adult (18–65 years old) and pediatric (0–9 years old) populations of 100 subjects each, comprising an equal proportion of male and female subjects. Physiologic parameters for the virtual adult population were generated based on the physiology of an average white American, as described in the 1997 National Health and Nutrition Examination Survey.

Age-relevant physiologic data from the International Commission on Radiological Protection were used to generate the virtual pediatric population.[20] Human β-tubulin isotype class I (TUBB) was selected to represent overall β-tubulin binding for this model, as it is both highly expressed and present in most human tissues.[21] Gene expression levels of CYP3A4/5, P-gp, and TUBB were obtained from UNIGENE and E-GEOD databases using the PK-Sim built-in database query. CYP3A4 expression was adjusted for age using the built-in PK-Sim ontogeny function. The equation for CYP3A4 ontogeny in the liver used in PK-Sim is

$$A = PMA^n / (A_{0.5}^n + PMA)$$

where PMA is the postmenstrual age in weeks; A is the activity at PMA; $A_{0.5}$ is the PMA at 50% activity compared with the

Table 1 Vincristine parameters used for the adult and pediatric PBPK models

Parameter		Value		Source
Molecular weight, g/mol		824.958		PubChem
Solubility, mg/L		2.27		
LogP		2.82		Hansch *et al.* (1995)[40]
pK$_a$		5.00 and 7.4		Owellen *et al.* (1977)[41]
f_u		0.51 (α-1-acid glycoprotein)		Mayer and St-Onge (1995)[36]
Metabolism		**rhCYP3A4**	**rhCYP3A5**	Dennison *et al.* (2006)[25]
	V$_{max}$ (pmol/min/pmol enzyme)	0.9	8.1	
	K$_m$ (μM)	19.8	14.3	
P-gp transport	J$_{max}$ (pmol/mL/min)	**Initial**	**Optimized**	Experimental
		416.1	416.1	
	K$_m$ (μM)	17.1	17.1	
Specific binding to β-tubulin		**Initial**	**Optimized**	Initial estimates for vinblastine–tubulin binding by Lobert *et al.* (1996)[22]
	k_{off} (1/s)	8.30×10^{-3}	1.93×10^{-3}	
	K$_D$ (μM)	0.05	0.05	
	Relative TUBB expression (μM)	1.00	1.00 (adult) 4.90 (pediatric)	UNIGENE and E-GEOD (PK-Sim database query)

f_u, unbound fraction; J$_{max}$, maximal rate of transport mediated by P-gp; K$_D$, dissociation constant for binding of vincristine to β-tubulin; K$_m$, Michaelis-Menten constant; k_{off}, dissociation rate constant for binding of vincristine to β-tubulin; LogP, partition coefficient; PBPK, physiologically based pharmacokinetic; P-gp, P-glycoprotein; PK, pharmacokinetic; rhCYP3A4 and rhCYP3A5, recombinant human CYP3A4 and CYP3A5; TUBB, human β-tubulin isotype class I; V$_{max}$, maximum rate of metabolism for CYP3A-mediated metabolism of vincristine.

PK-Sim Ontogeny Database version 7.3, an *n* of 3.331 and $A_{0.5}$ of 73.019 is used by the PK-Sim software.

Rate constants for β-tubulin binding of vincristine have not been determined previously, as once bound to tubulin, the vincristine–tubulin dimers associate and form microstructures that interfere with light-scatter methods of determining binding and dissociation constants.[22] Therefore, published constants (k_{off}, K$_D$) for another vinca alkaloid of a similar chemical structure, vinblastine (**Figure 1**), were used and optimized by parameter estimation.

Parameter estimation was performed using the built-in PK-Sim tool on the kinetic parameters for P-gp transport (K$_m$, J$_{max}$) and specific binding to β-tubulin (k_{off}, K$_D$, and relative expression of TUBB). A multiple optimization approach was used with randomized start values.

Model evaluation

Model performance was evaluated by comparing simulated plasma concentration-time profiles (population mean and 95% confidence interval (CI)) to observed concentration data. Models were accepted if simulated concentration-time profiles fit the overall shape of observed profiles, the majority of observed concentration data fell within the 95% CI for simulated data, and the simulated PK parameters were within two fold of the observed parameters.

Mean simulated adult PK parameters were compared with published experimental PK parameters derived from clinical studies of patients with cancer.[17–19] Mean simulated pediatric PK parameters were compared with the pediatric PK results from 25 children (0–12 years; Newcastle University).[23] Model robustness was further evaluated by comparing model simulations to additional published PK studies in which PK parameters (but not concentration data) were available.

Sensitivity analyses

Sensitivity analyses were performed using the PK-Sim tool to evaluate the effect of the metabolism (CYP3A4 and CYP3A5 K$_m$, maximum rate of metabolism (V$_{max}$), and expression), P-gp efflux (K$_m$, J$_{max}$, and expression), and tubulin-binding (k_{off}, K$_D$, and TUBB expression) input parameters on performance of the adult PBPK model. These three parameters were selected for sensitivity analyses as potential significant contributors to vincristine distribution and clearance. Input values were evaluated with over a 100% variation range (i.e., two fold) to determine the impact on the simulated PK parameters (AUC, CL, and volume of distribution (V$_D$)).

RESULTS
PBPK model for vincristine disposition in adults after i.v. administration

The whole-body PBPK model structure is shown in **Figure 1a**. Tissue to plasma partition coefficients were determined in PK-Sim using a method described by Schmitt.[24]

In vitro kinetic constants (K$_m$ and V$_{max}$) for the formation of the vincristine metabolite M1 by recombinant CYP3A4 and CYP3A5 were used.[25] Vincristine is metabolized by both CYP3A4 and CYP3A5, and the intrinsic clearance of vincristine by CYP3A5 is ~12-fold higher than by CYP3A4, despite similar affinity of both enzymes for vincristine.[25] Gene and protein expression of CYP3A4, but not CYP3A5, are age dependent and follow a pattern of ontogeny.[12] CYP3A5 is not highly expressed except in those with a specific genetic polymorphism.

Kinetic constants for P-gp efflux of vincristine in MDCK1-MDR1 cells, determined experimentally in this study, were used for initial modeling. Although vincristine is well known as a substrate of P-gp, kinetic parameters of its efflux have
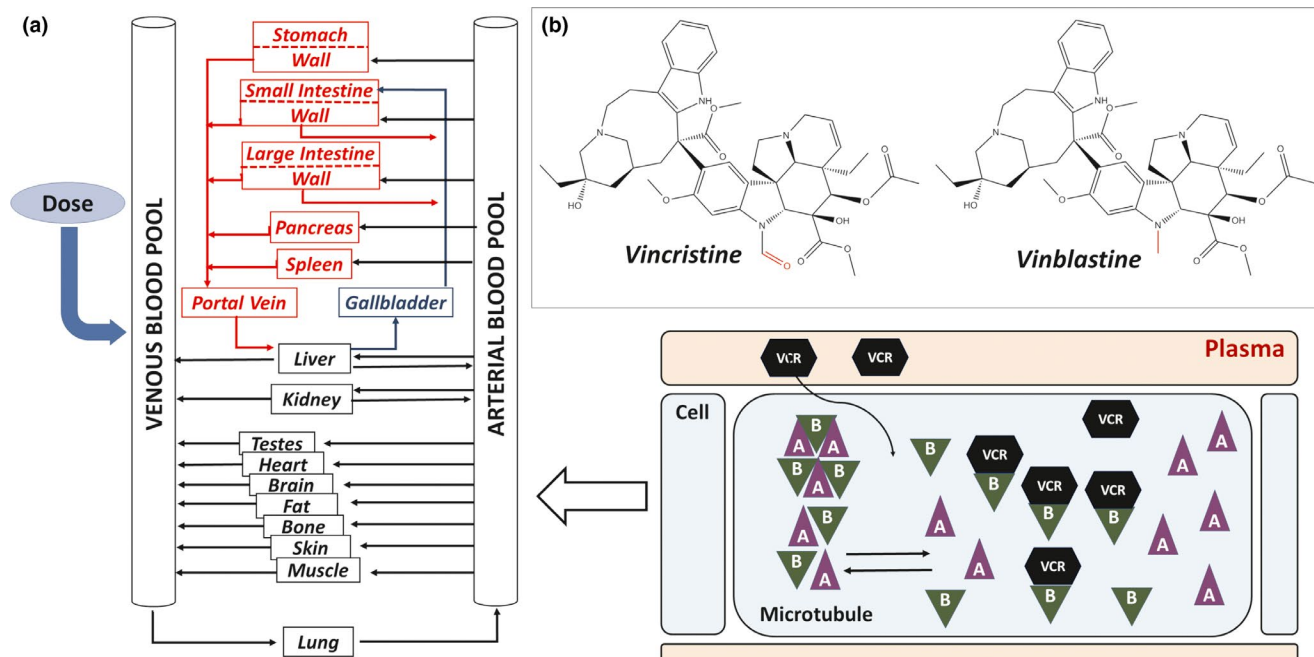
Figure 1 Whole-body physiologically based pharmacokinetic (PBPK) model for vincristine. (**a**) The model structure simulated by PK-Sim software package was adapted from Willmann et al. [42] The model includes simulation of the specific protein binding of vincristine to β-tubulin within the cellular compartment. Microtubule structures within the cell, comprising units of α-tubulin (represented by the triangles marked A) and β-tubulin subunits (represented by the triangles marked B), exchange subunits with an intracellular pool of unbound α-tubulin and β-tubulin, respectively. Vincristine enters the cell by passive diffusion and binds to the free intracellular β-tubulin.[43] The chemical structures of vincristine and vinblastine are inset in (**b**), with differences between structures noted in red.

not previously been reported. Kinetic studies of P-gp efflux are often performed *in vitro* using inside-out membrane vesicle systems overexpressing MDR1; however, it is difficult to achieve adequate intravesicular concentrations of lipophilic compounds such as vincristine for evaluation.[26,27] The permeability (P_{app}) of vincristine (10 μM) across MDCKII-MDR1 monolayers is sevenfold greater in the BL to AP direction (157 nm/s) than in the AP to BL direction (22 nm/s), consistent with AP efflux. Secretory transport of vincristine was significantly attenuated by GW918, an inhibitor of P-gp, decreasing the efflux ratio ($P_{app, BL to AP}/P_{app, AP to BL}$) from 7.1 to 1.5, providing evidence that the AP efflux of vincristine is mediated by P-gp. An apparent J_{max} of 46.6 pmol/min and K_m of 17.1 μM was obtained for vincristine flux mediated by P-gp ($R^2 = 0.862$). Based on the surface growth area for each Transwell (1.12 cm^2) and average cell yield listed by the manufacturer (1.12×10^6 cells; Corning Guidelines for Use: Transwell Permeable Supports), the J_{max} was estimated to be 416 pmol/min/million cells.

The adult PBPK model for vincristine that incorporates CYP3A4/5 metabolism, P-gp efflux, and specific binding to β-tubulin adequately described the observed concentration data (**Table 1 and Figure 2**). *In vitro* metabolism and transport kinetics are scaled to organs by the following equation by PK-Sim:

$$V_{max,organ} = k_{cat} \cdot SF \cdot e_{rel,organ} = k_{cat,s} \cdot e_{rel,organ}$$

in which $V_{max,organ}$ is the tissue-specific maximum velocity, k_{cat} is the catalytic rate constant (1/min), SF is the organ-specific scaling factor (μmol/L), e_{rel} is the relative expression of the enzyme or transporter protein, $e_{rel,s}$ is the apparent catalytic rate constant, and E_o is the enzyme or transporter concentration in the organ (μmol/L).

For initial model building and optimization, an i.v. infusion (15 minutes) of 2 mg vincristine was simulated to match the
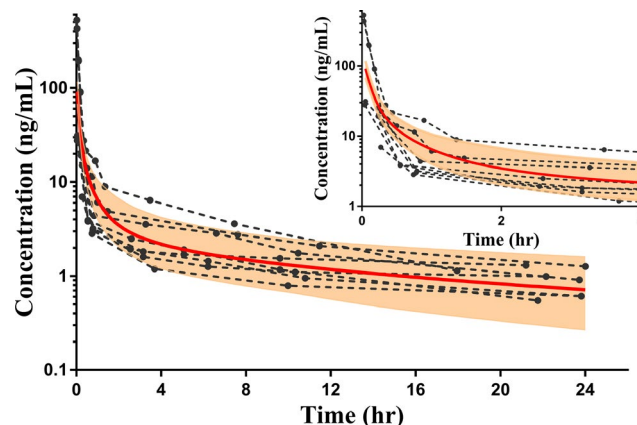

Figure 2 Simulation of vincristine concentration vs. time curve from 0 to 24 hours following a single i.v. dose of vincristine (2 mg) in a virtual adult population (*N* = 100). The solid red line represents the simulated mean, and the shaded area is the 95% confidence interval. The dotted lines represent the observed vincristine concentration vs. time profiles for 10 adults, extracted from publications by GetData.[17,44] The inset panel shows the concentration vs. time curve for 0–4 hours only.

dosing regimen of the observed clinical study that provided concentration data.[19] A majority of these observed concentration data were within the 95% CI of simulated vincristine plasma concentrations. To further evaluate the adult PBPK model, doses of 2 mg vincristine given by i.v. bolus and 60-minute infusion were also used in order to evaluate simulated PK parameters as compared with those published in two other studies.[18,28] Overall, the adult PBPK model predicted PK parameters (AUC, terminal half-life ($t_{1/2}$), V_D, and CL) well within a twofold margin of published parameters from all three PK studies (**Table 2**).

PBPK model for vincristine disposition in children after i.v. administration

The adult PBPK model for vincristine disposition was initially adapted to develop a pediatric model by incorporating age-related physiological differences, including the ontogeny of CYP3A4 expression. Although vincristine is also metabolized by CYP3A7, this enzyme is a fetal isoform that is not present after 6 months postnatal age.[12,25] Therefore, kinetic parameters for CYP3A4 and CYP3A5, but not CYP3A7, were included in the model. However, the simulation showed that vincristine distribution was not well described by the model (**Figure 3**). Despite incorporating the tubulin-binding parameters (k_{off}, K_D) optimized in the adult PBPK model, the pediatric PBPK model overpredicted vincristine concentrations relative to the observed concentrations. The overprediction error was greatest with the concentrations in the first 4 hours after dose, suggesting that the extent of distribution of vincristine was being underpredicted in the virtual pediatric population. Age-related differences in the expression of CYP3A4 and P-gp proteins do not explain the overprediction of vincristine concentrations by the model, as they would be expected to impact the clearance of vincristine and not its distribution.[14]

Differences in specific binding to β-tubulin were considered potential factors affecting the distribution of vincristine in children. Expression of TUBB was evaluated, because it is not known whether the expression of β-tubulin isotypes is different in children compared with adults. To evaluate the effect of relative expression of TUBB on the distribution of vincristine in the virtual pediatric population, the pediatric expression of TUBB was varied up to 150-fold of the adult reference concentration and the PK parameters were simulated. Linear regression analysis demonstrated that in the simulated pediatric population, the V_D of vincristine is significantly correlated with TUBB concentration ($P < 0.0001$). Parameter estimation was also performed using adult relative expression of TUBB to optimize pediatric TUBB expression. Surprisingly, model optimization suggested that simulating a higher expression of TUBB in children (~4.9-fold of adult expression) improved predictions. Specifically, predictions of vincristine concentrations in the distribution phase as well as prediction of pediatric V_D and $t_{1/2}$ improved significantly, although the AUC was underestimated to a greater extent (**Figure 3b and Table 3**). Following this adaptation, the pediatric model adequately described the observed pediatric concentration data for vincristine. PK parameters

Table 2 Comparison of experimental mean vs. simulated PK parameters of vincristine in the adult population

Source	Patient population	N	Dose	AUC$_{0-\infty}$ (ng*hour/mL)			t$_{1/2}$ (hour)			V$_D$ (L/kg)			CL (L/hour)		
					Fold difference	% Error^a		Fold difference	% Error		Fold difference	% Error		Fold difference	% Error
Model simulation	Adult, virtual population	100	2 mg, 15 min i.v. infusion	76.5	–	–	19.6	–	–	6.4	–	–	29.1	–	–
Villikka et al. (1999)[19]	Malignant brain tumors	6	2 mg, 15 min i.v. infusion	65.1	1.2	–17%	12.7	1.5	–54%	12.9	0.5	50%	34.1	0.9	15%
Fedeli et al. (1989)[28c]	Solid tumors	14	2 mg, i.v. bolus	48.3	1.6	–58%	21.7	0.9	10%	11.4	0.6	44%	35.4	0.8	18%
Model simulation	Adult, virtual population	100	2 mg, 60 min i.v. infusion	116.1	–	–	17.9	–	–	5.8	–	–	24.1	–	–
Yan et al. (2012)[18d]	Advanced solid tumors	6	2 mg, 60 min i.v. infusion	140.3	0.8	17%	16.0	1.1	–12%	5.0	1.2	–16%	14.6	1.7	–65%

AUC$_{0-\infty}$, area under the concentration-time curve from zero to infinity; CL, clearance; PK, pharmacokinetic; t$_{1/2}$, terminal half-life; V$_D$, volume of distribution.
^{a}Percentage error = (observed – simulated)/observed * 100.
^{b}V$_D$ and CL values for model simulation calculated based on average virtual population body mass of 77 kg.
^{c}V$_D$ and CL values from Fedeli et al.[28] converted based on mean patient BSA of 1.67 m^2 and weight (65.21 kg).
^{d}V$_D$ value from Yan et al.[18] converted based on median patient weight of 64 kg (mean not reported).
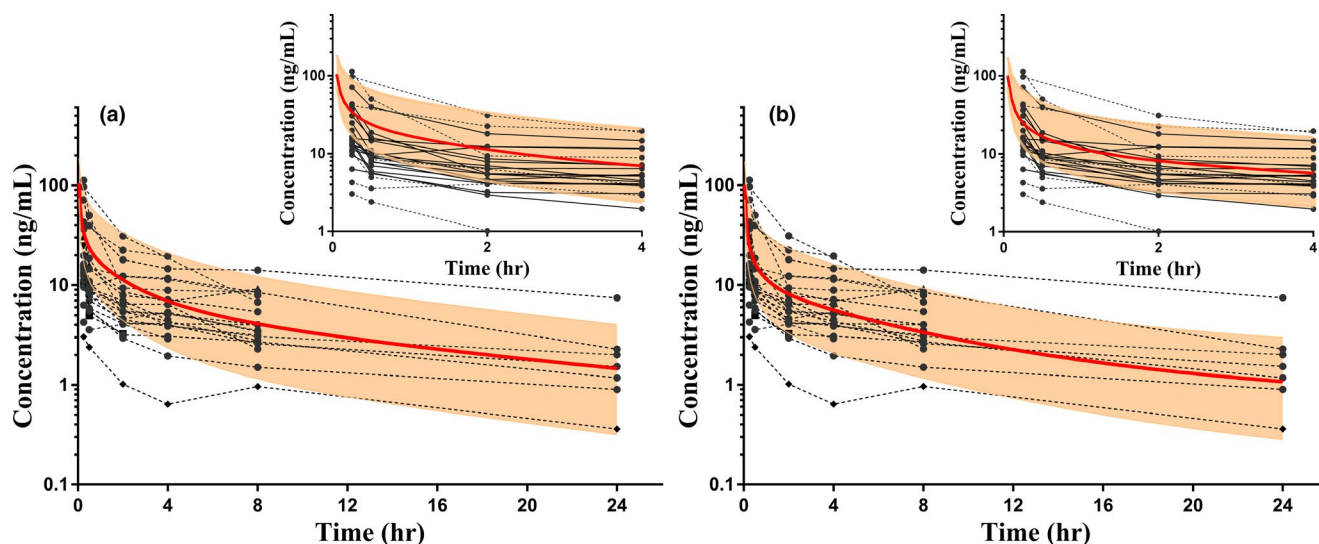
Figure 3 Simulations of vincristine concentration vs. time in the virtual pediatric population (*N* = 100) with observed concentration data of 25 children, aged 0–12 years. The solid red lines represent the simulated mean, and shaded areas represent the 95% confidence interval (CI). Observed concentrations (circles connected by dotted lines) have been normalized to the dose (mg) received. (**a**) The pediatric population simulation with physiologically based pharmacokinetic model, using adult expression levels of human β-tubulin isotype class I (TUBB). Relative TUBB expression in the virtual pediatric population was optimized by parameter estimation. As shown in (**b**), a higher expression of TUBB (4.9-fold increase relative to adult expression) improved predictions of pediatric vincristine concentrations, and more concentrations fall within the 95% CI compared with (**a**), particularly in the first 4 hours after dose. The inset panels in (**a**) and (**b**) show the concentration vs. time curves for 0–4 hours only.

were also predicted within a twofold margin of published parameters (**Table 3**).

Sensitivity analyses

Sensitivity analyses demonstrated that simulated adult vincristine area under the concentration-time curve from zero to infinity ($AUC_{0-\infty}$), $t_{1/2}$, and CL are sensitive to CYP3A4 V_{max} and CYP3A4 expression (**Table 4**). A 100% increase in CYP3A4 relative expression decreased AUC and $t_{1/2}$, and increased CL by >25%, indicating that CYP3A4 expression was an important parameter in the model for predicting vincristine exposure and clearance. The PK parameters were not sensitive to CYP3A5 V_{max} and relative expression in the model.

Changes in K_m, V_{max}, and relative expression of P-gp did not impact PK parameters; PK parameters changed by <10% when these input parameters were increased by 100%.

The K_D of tubulin binding to vincristine, as well as relative expression of TUBB, had a substantial impact on $AUC_{0-\infty}$, $t_{1/2}$, and CL as well as vincristine V_D. A 100% increase in K_D caused an increase in $AUC_{0-\infty}$ by 20% and a decrease in $t_{1/2}$, V_D, and CL by 13%, 34%, and 21%, respectively. Increasing the relative expression of TUBB by 100% had the opposite effect, decreasing $AUC_{0-\infty}$ by 20% but increasing $t_{1/2}$, V_D, and CL by 30%, 50%, and 19%, respectively. In contrast, PK parameters were not sensitive to changes in the k_{off} value.

DISCUSSION

Due to ethical considerations, development of pediatric drugs typically relies upon PK studies conducted in adults

to arrive at safe and effective doses in children. Subsequent pediatric dose selection, PK predictions, and predictions of drug–drug interactions are thus extrapolated from adult data, adjusted by allometric scaling. However, allometric scaling does not address developmental changes in hepatic function, renal function, organ sizes, or total body composition, nor does it account for the ontogeny of drug metabolizing enzymes or drug transporters. For example, the expression of CYP3A4 and the hepatic efflux transporter P-gp demonstrates patterns of ontogeny that could impact the disposition of substrate drugs in infants and younger children.[12,14] Bottom-up PBPK modeling provides a more rigorous approach to predict pediatric PK parameters. In this approach, an adult PBPK model is first developed and validated using available clinical PK data, then adapted to a pediatric PBPK model by incorporating *in vitro* metabolism/transport data, generated using relevant pediatric tissues, age-related changes in physiological parameters, and the expression of drug-metabolizing enzymes and transporters. For drugs such as voriconazole and sildenafil that are cleared predominantly by oxidative metabolism, we previously demonstrated that mechanistic PBPK modeling approaches can be used to predict PK in children and premature neonates, respectively.[10,11]

In the present study, the objective was to apply this PBPK modeling approach to vincristine, which is cleared via P-gp-mediated hepatic efflux and CYP3A-mediated hepatic oxidative metabolism. Vincristine is used as the first-line therapy in common pediatric leukemias such as ALL and in pediatric solid tumor cancer treatment. Vincristine exhibits high interpatient variability, and there is limited availability of pediatric PK data. In some studies, but not others, correlations have been shown between vincristine PK parameters

Table 3 Comparison of experimental mean vs. simulated PK parameters of vincristine in the pediatric population

Source	Patient population	N	Dose (mg/m²)	AUC$_{0-\infty}$ (ng*hour/mL)			t$_{1/2}$ (hour)			V$_D$ (L/kg)			CL (L/hour)		
					Fold difference	% Error[a]		Fold difference	% Error		Fold difference	% Error		Fold difference	% Error
Model simulation, adult TUBB expression	Pediatric (0–12 years) virtual population	100	1	149.6	–	–	12.5	–	–	5.6	–	–	8.7	–	–
Final model simulation, 4.9-fold increase in TUBB expression	Pediatric (0–12 years) virtual population	100	1	118.6	–	–	15.6	–	–	8.6[b]	–	–	10.7	–	–
Pediatric patients with Wilms tumor	Pediatric (0–12 years)	23[c]	1.5[d]	186.4[e]	0.6	36.4%	16.0[e]	1.0	2.5%	9.8[e,f]	0.9	12.2%	10.4[e]	1.0	–2.9%

AUC$_{0-\infty}$, area under the concentration-time curve from zero to infinity; CL, clearance; PK, pharmacokinetic; t$_{1/2}$, terminal half-life; TUBB, human β-tubulin isotype class I; V$_D$, volume of distribution.

[a] Percentage error = (observed – simulated)/observed * 100.
[b] V$_D$ value calculated based on average pediatric body mass of virtual subjects, 26.4 kg (N = 100).
[c] Plasma concentration data were available for 25 pediatric subjects. However, PK analyses could not be completed for two subjects due to insufficient number of concentrations.
[d] Dose reduced by one-third if under 12 kg.
[e] Calculated using plasma concentrations normalized to dose (mg).
[f] V$_D$ value converted based on average pediatric body mass of study subjects, 16.4 kg (N = 25).

and clinical outcome as well as risk of the dose-limiting toxicity, peripheral neuropathy.[5–7] Therefore, we believe that it is important to develop an adult mechanistic PBPK model of vincristine that can be validated using available clinical PK data and adapt it to a pediatric PBPK model that can guide dosing of the drug in pediatric patients with ALL and solid tumors.

Simulations with the initial adult model revealed that the distribution phase was not well predicted. Hence, we reasoned that because vincristine exerts its antimitotic effects by binding to intracellular β-tubulin subunits, this intracellular binding may also impact the overall distribution of vincristine. By incorporating the binding of vincristine to β-tubulin, simulated plasma concentrations were adequately described in comparison to the observed concentration data, with the majority of observed data points falling within the 95% CI. The improved PBPK model was able to predict adult PK parameters of vincristine (AUC, t$_{1/2}$, V$_D$, and CL) within a twofold margin of the observed parameters from three published PK studies (**Table 2**). These results suggested that binding to β-tubulin might have a key role in vincristine distribution.

Sensitivity analyses were performed to evaluate the relevance of the key processes that were incorporated in the PBPK model as determinants of the PK behavior of vincristine. These analyses demonstrated that CYP3A4 V$_{max}$ and expression influenced simulated adult vincristine clearance and exposure (AUC), consistent with the reported predominantly CYP3A4-mediated metabolism of vincristine.[25] For example, a 100% increase in CYP3A4 relative expression decreased AUC and t$_{1/2}$ and increased CL by >25% (**Table 4**). Although it has been reported that CYP3A5 plays a larger role than CYP3A4 in the metabolism of vincristine, changes in CYP3A5 V$_{max}$ and expression showed less impact on vincristine PK parameters. This may be due to low or no CYP3A5 expression in the patient population providing the observed concentration data and PK parameters. Based on the location of the studies, the pediatric population and the adult populations in the two published studies were presumed to be a majority of white and East Asian patients.[19,28] The frequency of the nonfunctional variant, *CYP3A5*3* allele (CYP3A5 nonexpresser), is 92–94% and 71–75% for a white European and East Asian population, respectively.[29] Contrary to expectations, sensitivity analyses of P-gp K$_m$ and J$_{max}$ in the adult PBPK model indicated that AUC, CL, or V$_D$ parameters did not change even upon a 100% increase in these kinetic parameters. Thus, it seems that biliary efflux via P-gp may not be the critical factor in defining vincristine hepatic clearance. Studies utilizing suspended cryopreserved human hepatocytes also indicate that the rate-limiting factor is not efflux via P-gp, which is consistent with the conclusion reached based on the sensitivity analyses but suggests a possible role of BL organic anion transporter proteins[27] in rate-limiting uptake into hepatocytes.

The importance of intracellular binding of vincristine to tubulin is supported by the sensitivity of PK parameters to changes in the K$_D$ and TUBB values. Theoretical increases in the affinity for binding of vincristine to tubulin subunits

Table 4 Sensitivity analyses of the effect of CYP3A4, CYP3A5, P-gp, and β-tubulin-binding parameters on vincristine PKs in adults

		$AUC_{0-\infty}$	$t_{1/2}$	V_D	CL
CYP3A4	rhCYP V_{max}	−0.35	−0.36	−0.01	0.34
	Relative expression	−0.26	−0.26	−0.00139	0.25
CYP3A5	rhCYP V_{max}	−0.04	−0.04	0.00599	0.04
	Relative expression	−0.02	−0.02	−0.0002	0.02
P-gp	K_m	−0.05	−0.00958	0.04	0.05
	V_{max}	0.05	0.0095	−0.04	−0.05
	Relative expression	−0.05	−0.00943	0.04	0.05
Binding to β-tubulin	K_D	0.20	−0.13	−0.34	−0.21
	k_{off}	−0.00043	−0.00243	−0.002	0.000429
	TUBB relative expression	−0.20	0.30	0.50	0.19

$AUC_{0-\infty}$, area under the concentration-time curve from zero to infinity; CL, clearance; P-gp, P-glycoprotein transporter; PKs, pharmacokinetics; $t_{1/2}$, terminal half-life; TUBB, human β-tubulin isotype class I; V_D, volume of distribution; V_{max}, maximal rate of metabolism.
Sensitivity analyses using the built-in PK-Sim tool were performed to evaluate effect of input parameters on performance of the adult physiologically based pharmacokinetic model. Input values were evaluated over a 100% variation range to determine impact on simulated adult PK parameters (e.g., a 100% increase in CYP3A4 relative expression decreased $AUC_{0-\infty}$ and $t_{1/2}$ by >25%). Overall, the analyses demonstrated that PK parameters are sensitive to changes in CYP3A4 relative expression, K_D of β-tubulin binding to vincristine, and relative expression of TUBB.

(by decreasing K_D) or in the expression of TUBB would lead to increased intracellular binding. In both cases, sensitivity analyses suggest that an increase in intracellular binding would result in more extensive distribution (increase in V_D) and decreased plasma levels (AUC) of vincristine. *In vitro*, the intracellular accumulation of vincristine is strongly correlated with β-tubulin expression.[30] In mice and dogs, tissue concentrations of vincristine and tissue-to-plasma partition coefficients were also highly correlated with β-tubulin binding capacity, suggesting that β-tubulin could also play an important role in tissue distribution and accumulation of vincristine in humans.[31] Further corroboration of the importance of β-tubulin binding to the distribution of vincristine is provided by mechanistic modeling of the taxane docetaxel, which binds to a different site of the β-tubulin subunit. Published mouse PBPK models of docetaxel incorporated the specific binding of docetaxel to β-tubulin (K_D) and an estimated tubulin-binding capacity.[32,33] When tubulin-binding capacity was adjusted for organ size, the mouse PBPK model was successfully adapted to predict docetaxel PK in adult humans.[33] Although the ontogeny of β-tubulin expression is unknown, its expression and content vary by organ, as well as organ sizes, which are age dependent. Therefore, in addition to hepatic efflux by P-gp and metabolism by CYP3A enzymes, it is possible that the extent of intracellular binding to β-tubulin could differ in children vs. adults, due to differences in either β-tubulin expression or organ sizes.

The pediatric PBPK model was adapted from the adult model by incorporating age-related physiological differences, including the ontogeny of CYP3A4 expression (CYP3A5 expression is not age dependent[12]). Although the sensitivity analyses indicated that P-gp might not play a significant role in determining PK parameters of vincristine, the ontogeny of P-gp was also considered, as protein expression of P-gp is ~60% and 80% of adult levels in infants and children, respectively.[14] We also considered the binding of vincristine to the plasma protein α-1-acid glycoprotein (AAG),[34] as AAG levels increase with age.[35] Because vincristine is not extensively bound to AAG

(f_u 0.51) and AAG levels are lower in young children, this was not expected to explain the distribution of vincristine in children.[36] Surprisingly, model optimization suggested that simulating a higher relative expression of TUBB in children (4.9-fold higher than adult expression) improved predictions of vincristine concentrations. To our knowledge, the effect of age on tubulin expression has not previously been studied. We hypothesize that the greater extent of vincristine distribution observed in children compared with adults was likely due to the pediatric PK samples being sourced from patients with large solid tumors (i.e., Wilms tumor). Gene expression of β-tubulin subunits in 15 pediatric patients with Wilms tumor was at least two fold greater as compared with noncancerous adult kidney tissue.[37] Further *in silico* and *in vitro* studies are needed to understand the physiological basis for possible differences in tubulin binding that are associated with age.

There are two limitations of this study pertaining to the incorporation of β-tubulin into the PBPK models. First, published values for vinblastine were used as the initial estimates for *in vitro* binding of vincristine to β-tubulin, because binding parameters for vincristine have not been reported in the literature. Vincristine and vinblastine are structurally similar vinca alkaloids (**Figure 1**), with similar thermodynamics and binding parameters to several β-tubulin isotypes.[38] The vinblastine and vincristine equilibrium constants (K) for binding to tubulin subunits are similar (1.5×10^5 M^{-1} and 1.4×10^5 M^{-1}, respectively).[22] Published estimates of k_{off} for vinblastine binding to β-tubulin range from 0.006 to 0.0083 1/s.[22,39] In simulations with the adult PBPK model of vincristine, decreases in k_{off} by orders of magnitude were required to impact the simulation and decreased accuracy of the model predictions. Furthermore, a sensitivity analysis of k_{off} indicates that increasing this value by 100% does not impact simulated PK parameters of vincristine (**Table 4**). The value obtained for vincristine by parameter estimation, 0.00193 1/s, seems to be a reasonable estimate based on the published vinblastine k_{off} values. Second, expression of only one isotype of β-tubulin, TUBB, was used in the PBPK models due to its ubiquity in human

tissues, although there are eight human β-tubulin isotypes. Expression of these isotypes varies widely in the body; for example, isotypes IIa and IVa are expressed almost exclusively in neural tissue.[21] Further adaptation of the model to include additional isotypes of β-tubulin may be useful in understanding vincristine distribution to specific organs and tissues.

In summary, the mechanistic PBPK models developed in this study predict vincristine PK in adults and children upon i.v. administration. Notably, the models yield interesting mechanistic information about the key determinants of the PK parameters of vincristine that could not have been obtained through clinical studies. Specifically, the PBPK models suggest that CYP3A5 and P-gp, which were implicated in the clearance of vincristine from *in vitro* studies, do not play a significant role in the clearance of vincristine in either adults or children. Further, we found that intracellular binding had to be invoked in building the model to describe and predict the distribution phase of vincristine PK. In retrospect, the rationale for the importance of intracellular binding in vincristine PK is clear, because binding to β-tubulin is the mechanistic basis for the anticancer activity of this drug. To our knowledge, this is the first example in which intracellular binding has been incorporated into a pediatric PBPK model. Additionally, this study raises an interesting possibility that there may be age-related differences in the extent of intracellular binding to β-tubulin, leading to the corresponding differences in vincristine PK in these two populations. We believe that PBPK modeling of vincristine disposition in children will improve the prediction of PK parameters in pediatric patients, providing a useful tool to investigate the relationship between vincristine exposure and clinical outcomes without invasive monitoring of plasma drug concentrations.

Supporting Information. Supplementary information accompanies this paper on the *CPT: Pharmacometrics & Systems Pharmacology* website (www.psp-journal.com).

Table S1. Vincristine compound file.

Conflicts of Interest. The authors declared no competing interests for this work.

Author Contributions. C.M.L. and D.R.T. wrote the manuscript and designed research. C.M.L., G.V., and D.R.T. performed research. C.M.L., N.R.Z., G.V., and D.R.T. analyzed data.

1. Ward, E., DeSantis, C., Robbins, A., Kohler, B. & Jemal, A. Childhood and adolescent cancer statistics, 2014. *CA Cancer J. Clin.* **64**, 83–103 (2014).
2. Inaba, H., Greaves, M. & Mullighan, C. Acute lymphoblastic leukemia. *Lancet* **381**, 1–27 (2013).
3. Gidding, C.E.M., Kellie, S.J., Kamps, W. & De Graaf, SSN. Vincristine revisited. *Crit. Rev. Oncol. Hematol.* **29**, 267–287 (1999).
4. Carlson, K. & Ocean, A.J. Peripheral neuropathy with microtubule-targeting agents: occurrence and management approach. *Clin. Breast Cancer* **11**, 73–81 (2011).
5. Crom, W.R. *et al.* Pharmacokinetics of vincristine in children and adolescents with acute lymphocytic leukemia. *J. Pediatr.* **125**, 642–649 (1994).
6. Egbelakin, A., Ferguson, M.J., MacGill, E.A., Lehmann, A.S. & Renbarger, J.L. Increased risk of vincristine neurotoxicity associated with low CYP3A5 expression genotype in children with acute lymphoblastic leukemia. *Pediatr. Blood Cancer* **56**, 361–367 (2012).
7. Lönnerholm, G. *et al.* Vincristine pharmacokinetics is related to clinical outcome in children with standard risk acute lymphoblastic leukemia. *Br. J. Haematol.* **142**, 616–621 (2008).
8. Moriyama, B. *et al.* Adverse interactions between antifungal azoles and vincristine: review and analysis of cases. *Mycoses* **55**, 290–297 (2012).
9. Israels, T. *et al.* Malnourished Malawian patients presenting with large Wilms tumours have a decreased vincristine clearance rate. *Eur. J. Cancer* **46**, 1841–1847 (2010).
10. Zane, N.R. & Thakker, D.R. A physiologically based pharmacokinetic model for voriconazole disposition predicts intestinal first-pass metabolism in children. *Clin. Pharmacokinet.* **53**, 1171–1182 (2014).
11. Zane, N.R. Predicting pharmacokinetic behavior and dose of sildenafil and voriconazole in neonatal and pediatric populations by in vitro metabolism and PBPK modeling (Doctoral dissertation). *Retrieved from Carolina Digit Repos* (2015).
12. Stevens, J.C. *et al.* Developmental expression of the major human hepatic CYP3A enzymes. *J. Pharmacol. Exp. Ther.* **307**, 573–582 (2003).
13. Gidding, C.E., Meeuwsen-de Boer, G.J., Koopmans, P., Uges, D.R., Kamps, W.A. & de Graaf, S.S. Vincristine pharmacokinetics after repetitive dosing in children. *Cancer Chemother. Pharmacol.* **44**, 203–209 (1999).
14. Prasad, B. *et al.* Ontogeny of hepatic drug transporters as quantified by LC-MS/MS proteomics. *Clin. Pharmacol. Ther.* **100**, 362–370 (2016).
15. Troutman, M.D. & Thakker, D.R. Efflux ratio cannot assess P-glycoprotein-mediated attenuation of absorptive transport: asymmetric effect of p-glycoprotein on absorptive and secretory transport across caco-2 cell monolayers. *Pharm. Res.* **20**, 1200 (2003).
16. Gao, J., Murase, O., Schowen, R.L., Aube, J. & Borchardt, R.T. A functional assay for quantitation of the apparent affinities of ligands of P-glycoprotein in caco-2 cells. *Pharm. Res.* **18**, 171–176 (2001).
17. Sethi, V.S. *et al.* Pharmacokinetics of vincristine sulfate in adult cancer patients. *Cancer Res.* **41**, 3551–3555 (1981).
18. Yan, Z. *et al.* Pharmacokinetic characteristics of vincristine sulfate liposomes in patients with advanced solid tumors. *Acta Pharmacol. Sin.* **33**, 852–858 (2012).
19. Villikka, K., Kivistö, K.T., Mäenpää, H., Joensuu, H. & Neuvonen, P.J. Cytochrome P450-inducing antiepileptics increase the clearance of vincristine in patients with brain tumors. *Clin. Pharmacol. Ther.* **66**, 589–593 (1999).
20. Valentin, J. Basic anatomical and physiological data for use in radiological protection. *Ann. ICRP* **32**, 5–265 (2002).
21. Leandro-García, L.J. *et al.* Tumoral and tissue-specific expression of the major human beta-tubulin isotypes. *Cytoskeleton* **67**, 214–223 (2010).
22. Lobert, S., Vulevic, B. & Correia, J.J. Interaction of vinca alkaloids with tubulin: a comparison of vinblastine, vincristine, and vinorelbine. *Biochemistry* **35**, 6806–6814 (1996).
23. Peters, S.P. *et al.* Tiotropium bromide step-up therapy for adults with uncontrolled asthma. *N. Engl. J. Med.* **363**, 1715–1726 (2010).
24. Schmitt, W. General approach for the calculation of tissue to plasma partition coefficients. *Toxicol. Vitr.* **22**, 457–467 (2008).
25. Dennison, J.B., Kulanthaivel, P., Barbuch, R.J., Renbarger, J.L., Ehlhardt, W.J. & Hall, S.D. Selective metabolism of vincristine in vitro by CYP3A5. *Drug Metab. Dispos.* **34**, 1317–1327 (2006).
26. Giacomini, K.M., Huang, S., Tweedie, D.J. & Benet, L.Z. Membrane transporters in drug development. *Nat. Rev. Drug Discov.* **9**, 215–236 (2010).
27. Nicolaï, J. *et al.* Role of the OATP transporter family and a benzbromarone-sensitiveefflux transporter in the hepatocellular disposition of vincristine. *Pharm. Res.* **34**, 2336–2348 (2017).
28. Fedeli, L. *et al.* Pharmacokinetics of vincristine in cancer patients treated with nifedipine. *Cancer* **64**, 1805–1811 (1989).
29. Xie, H.-G., Wood, A.J., Kim, R.B., Stein, C.M. & Wilkinson, G.R. Genetic variability in CYP3A5 and its possible consequences. *Pharmacogenomics* **5**, 243–272 (2004).
30. Reichle, A., Diddens, H., Altmayr, F., Rastetter, J. & Andreesen, R. Beta-tubulin and P-glycoprotein: major determinants of vincristine accumulation in B-CLL cells. *Leuk. Res.* **19**, 823–829 (1995).
31. Wierzba, K., Sugiyama, Y., Okudaira, K., Iga, T. & Hanano, M. Tubulin as a major determinant of tissue distribution of vincristine. *J. Pharm. Sci.* **76**, 872–875 (1987).
32. Hudachek, S.F. & Gustafson, D.L. Incorporation of ABCB1-mediated transport into a physiologically-based pharmacokinetic model of docetaxel in mice. *J. Pharmacokinet. Pharmacodyn.* **40**, 437–449 (2013).
33. Bradshaw-Pierce, E.L., Eckhardt, S.G. & Gustafson, D.L. A physiologically based pharmacokinetic model of docetaxel disposition: from mouse to man. *Clin. Cancer Res.* **13**, 2768–2776 (2007).

34. Donigian, D.W. & Owellen, R.J. Interaction of vinblastine, vincristine, and colchicine with serum proteins. *Biochem. Pharmacol.* **22**, 2113–2119 (1973).

35. Maharaj, A.R., Gonzalez, D., Cohen-Wolkowiez, M., Hornik, C.P. & Edginton, A.N. Improving pediatric protein binding estimates: an evaluation of α1-acid glycoprotein maturation in healthy and infected subjects. *Clin. Pharmacokinet.* **57**, 577–589 (2018).

36. Mayer, L.D. & St.-Onge, G. Determination of free and liposome-associated doxorubicin and vincristine levels in plasma under equilibrium conditions employing ultrafiltration techniques. *Anal. Biochem.* **232**, 149–157 (1995).

37. Takahashi, M. *et al.* Gene expression profiling of favorable histology Wilms tumors and its correlation with clinical features. *Cancer Res.* **62**, 6598–6605 (2002).

38. Lobert, S., Frankfurter, A. & Correia, J.J. Energetics of vinca alkaloid interactions with tubulin isotypes: implications for drug efficacy and toxicity. *Cell Motil. Cytoskeleton* **39**, 107–121 (1998).

39. Gigant, B. *et al.* Structural basis for the regulation of tubulin by vinblastine. *Nature* **435**, 519–522 (2005).

40. Hansch, C. Exploring QSAR – Hydrophobic, Electronic, and Steric Constants. (American Chemical Society, Washington DC, 1995).

41. Owellen, R.J., Donigian, D.W., Hartke, C.A. & Hains, F.O. Correlation of biologic data with physico-chemical properties among the Vinca alkaloids and their congeners. *Biochem. Pharmacol.* **26**, 1213–1219 (1977).

42. Willmann, S., Lippert, J., Sevestre, M., Solodenko, J., Fois, F. & Schmitt, W. PK-Sim®: a physiologically based pharmacokinetic 'whole-body' model. *Biosilico* **1**, 121–124 (2003).

43. Wilson, L. & Jordan, M.A. New microtubule/tubulin-targeted anticancer drugs and novel chemotherapeutic strategies. *J. Chemother.* **16**, 83–85 (2014).

44. Villikka, K., Kivistö, K.T., Mäenpää, H., Joensuu, H. & Neuvonen, P.J. Cytochrome P450-inducing antiepileptics increase the clearance of vincristine in patients with brain tumors. *Clin. Pharmacol. Ther.* **66**, 589–593 (1999).